Radiation Protection Dosimetry (2008), Vol. 129, No. 1–3, pp. 261–264 doi:10.1093/rpd/ncn027
Advance Access publication 26 February 2008

CRITERIA TO OPTIMISE A DYNAMIC FLAT DETECTOR SYSTEM USED FOR INTERVENTIONAL RADIOLOGY

R. Simon[1,2], E. Vano[1,3,*], C. Prieto[1], J. M. Fernandez[1,3], J. M. Ordiales[1] and D. Martinez[1]
[1]Medical Physics Service. San Carlos University Hospital, 28040 Madrid, Spain
[2]Present address: Clinical University Hospital, 47005 Valladolid, Spain
[3]Radiology Department. Medicine School, Complutense University, 28040 Madrid, Spain

An analysis of the relationship between image quality and incident air kerma has been carried out for a dynamic flat detector X-ray system used for interventional radiology. A phantom of polymethyl methacrylate (PMMA) to simulate patients and two different image test objects, Leeds TOR 18FG and NEMA XR 21, were used to evaluate the quality of the obtained images. Measurements were made simulating clinical configuration with different PMMA thicknesses (16, 20, 24 and 28 cm), available fields of view of 22, 31, 42 and 48 cm (diagonal dimension), in the three default fluoroscopy modes and in one of the most used digital subtraction angiography image acquisition modes. The obtained results are being used to help in the optimisation of clinical procedures.

INTRODUCTION

New interventional X-ray systems offer to the users many configuration settings and operation modes. Sometimes, during the acceptance tests and the commissioning process, it is not possible to evaluate all the available modes of operation and to select the most appropriate initial settings. A compromise is typically adopted by the manufacturers, offering the settings already tested in other hospitals. In any case, clinicians should know the radiation dose required for the different imaging modes, to properly use the X-ray systems and to suggest some improvements, if necessary, in the initial settings. There still is not much experience with this process for dynamic flat detectors used in the new systems for interventional radiology[1]. This paper offers some experimental results obtained with a Philips Allura Xper FD20[2].

There are several test objects allowing the evaluation of image quality for fluoroscopy systems. The Leeds TOR 18FG test object is one of the most popular in Europe[3,4]. The NEMA XR 21[5,6] test object has been promoted in USA for similar image quality evaluations.

There are other more sophisticated numerical methods to evaluate image quality, but they are quite difficult to use in the routine work at the hospitals[7–9].

MATERIAL AND METHODS

An interventional Philips Integris Allura flat detector X-ray system Xper FD20[2] was employed for the measurements. A solid-state-detector, UNFORS Xi[10] was used to measure the dose at the entrance of the simulated patient without backscatter, the incident air kerma (IAK)[11]. The Unfors Xi system can simultaneously measure kVp, dose, dose rate, HVL, pulse, pulse rate, dose/pulse, time, waveform and filtration. It was placed inside the radiation beam, but not in the automatic exposure control (AEC) area. The system Xper FD20 permits to visualise and change this AEC area if necessary. It allows recording both digital subtraction angiography (DSA) images and fluoroscopy runs in DICOM format. This feature allows the numerical analysis of the fluoroscopy images.

Entrance air kerma to the detector was measured during the acceptance tests of the X-ray system. The technical specifications include these values with 20 cm of polymethyl methacrylate (PMMA) and the antiscatter grid on the beam, with 1195 mm focal spot to image receptor distance and 660 mm between the focal spot and the interventional reference point (Table 1).

The detector was placed on top of the table, without the mattress, at the entrance of the X-ray beam to a variable amount of PMMA phantom. An image object test was placed in the middle of the PMMA and at the isocentre of the X-ray system (to simulate clinical conditions). The flat detector (FD) was maintained at a distance of 5 cm from the upper part of the PMMA plates. This system configuration simulates a typical patient thickness for the X-ray system loading in routine clinical practice.

Measurements were made for 16, 20, 24 and 28 cm of PMMA for the different fields of view (FOV): 22, 31, 42 and 48 cm (diagonal dimensions) in the three available fluoroscopy modes (high, normal, low) and in DSA acquisition mode. The pixel size of the flat panel detector is 154 × 154 μm

*Corresponding author: eliseov@med.ucm.es

Table 1. Reference air kerma rate for different FOV and different fluoroscopy modes. (technical specifications).

FOV (cm)	Low (mGy/s)	Normal (mGy/s)	High (mGy/s)
22	0.19	0.46	0.57
31	0.13	0.33	0.42
42	0.1	0.27	0.34
48	0.08	0.23	0.27

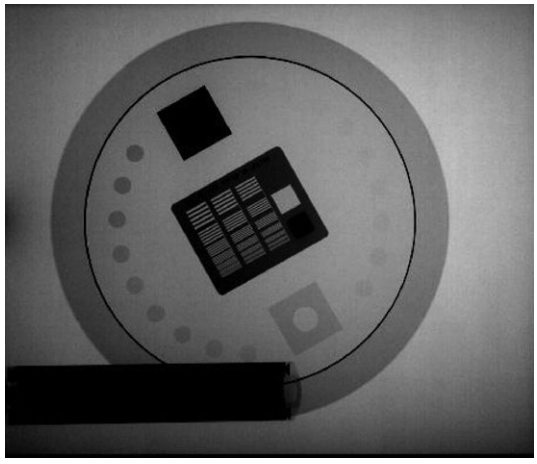

Figure 1. Leeds TOR 18FG. 20 cm PMMA, 42 cm FOV, DSA.

and the detective quantum efficiency is bigger than 65% at low spatial frequencies[2]. The selected default acquisition protocol was 'abdomen 2D' with a 'standard patient' (supposed to be 70 kg and 170 cm height). A special acquisition protocol was prepared by the Philips engineer, without post processing of the image (mainly edge enhancement and contrast harmonisation).

Two test objects were employed: Leeds TOR 18FG[4] (Figure 1) and NEMA XR 21[6] (Figure 2). The test object in the X-ray beam raises IAK and changes slightly the characteristics of the beam. This increase has been assessed for each test object separately.

Leeds TOR 18FG arranges 18 low-contrast circles, each one with different metal thickness, with an exponential decrease between them. NEMA XR 21 has four sets of holes of different diameters filled with different concentrations of iodine embedded in epoxy, with a linear decrease on them. Both phantoms include in the centre a standard bar metal pattern to analyse the high-contrast spatial resolution, with 16 series of bars in which the resolution goes from 0.5 to 5 line-pairs/mm.

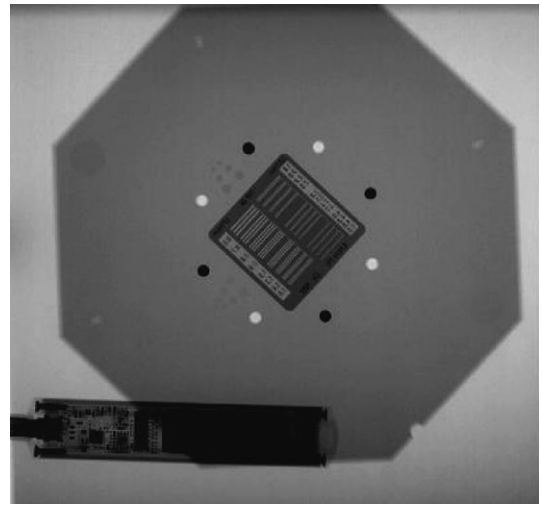

Figure 2. NEMA XR 21. 20 cm PMMA, 42 cm FOV, DSA.

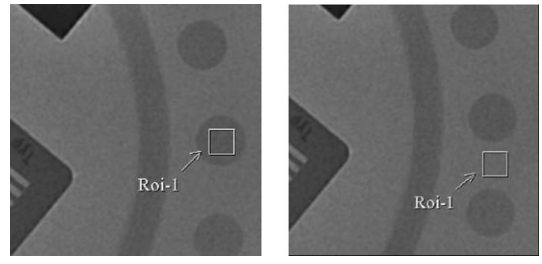

Figure 3. Example of ROIs considered for the calculations (CIR and BG).

Image quality was numerically analysed with the signal–noise ratio (SNR) in the higher-contrast circles of both test objects (in the case of NEMA, also in the biggest one). A region of interest (ROI) was drawn inside the analysed circle and another one on the surrounding area, on the background (BG) of the test object, near the circle (Figure 3). Different software can produce values of mean and standard deviation of pixels on an ROI. Osiris 4.19[12] was employed for this.

In the context of the signal detection theory, the SNR is proportional to a ratio of the magnitude of the difference between the mean values of some quantity under two conditions that are to be distinguished, to a measure of the magnitude of statistical variation in that difference[13].

$$\mathrm{SNR} = (\mathrm{BG} - \mathrm{CIR})\left(\frac{1}{2}(S\mathrm{CIR}^2 + S\mathrm{BG}^2)\right)^{-\frac{1}{2}}$$

- BG is the mean value of the pixel content in a selected ROI near the circle of study (test object's background)
- CIR is the mean value of the pixel content in a selected ROI inside the circle of study
- S is the standard deviation for the pixel content in the selected ROI of study

Several images of each series were selected, discarding the first ones, allowing the system being completely adjusted. The main source of error was not the ROI selection. The variability between the different images selected (after discarding the first ones) was more important. The average and the standard deviations of the SNRs were obtained. It was assumed that they fit a normal distribution and presented the confidence interval of 95%.

RESULTS

Inserting either test object increases the dose differently because the AEC does not adjust the X-ray system in the same way. We noticed not much difference in IAK when using the two test objects. The NEMA test object yields an increase in IAK, with respect to the Leeds one, of less than 15%.

Doing similar measurements with an ionisation chamber instead of a solid-state detector, the entrance surface air kerma (ESAK) including backscatter resulted in an increase of approximately 30% (ratio between ESAK and IAK in our experimental conditions is approximately 1.3).

When going from low to normal or high fluoroscopy mode (Table 2), IAK is increased by a factor of 1.6 and 2.7 with the Leeds test, and 1.5 and 2.4 with the NEMA test. SNR is increased by a factor of 1.3 and 1.9 with the Leeds test and 1.7 and 2.1 with the NEMA test, maintaining other conditions constant.

When magnification is applied in normal fluoroscopy mode, and FOV is changed from 48 cm to 42, 31 or 22 cm (Table 3), IAK is multiplied by factors of 1.7, 1.8 and 2.4 when the Leeds test was used and 1.3, 1.8, 2.1 when the NEMA one was used, nevertheless no big changes in SNR are seen.

Table 2. Variation of IAK and SNR in the different fluoroscopy modes with different test objects for 20 cm of PMMA and a 22 cm FOV.

Fluoroscopy mode	LEEDS TOR 18FG		NEMA XR 21	
	IAK (μGy/fr)	SNR	IAK (μGy/fr)	SNR
Low	14.7	1.76 ± 0.16	16.7	0.93 ± 0.09
Normal	23.2	2.29 ± 0.10	25.0	1.59 ± 0.22
High	39.2	3.3 ± 0.4	40.5	1.96 ± 0.06

Table 3. Variation of IAK and SNR for different FOV with different test objects, 20 cm of PMMA and in normal fluoroscopy mode.

FOV (cm)	LEEDS TOR 18FG		NEMA XR 21	
	IAK (μGy/fr)	SNR	IAK (μGy/fr)	SNR
22	23.2	2.29 ± 0.10	25.0	1.59 ± 0.22
31	14.0	2.62 ± 0.24	19.1	1.54 ± 0.24
42	13.2	2.61 ± 0.21	13.6	1.5 ± 0.5
48	9.8	2.61 ± 0.22	11.9	1.45 ± 0.23

Table 4. Variation of IAK and SNR with the amount of PMMA for different test objects in normal fluoroscopy mode and a 31 cm FOV.

PMMA (cm)	LEEDS TOR 18 FG		NEMA XR21	
	IAK (μGy/fr)	SNR	IAK (μGy/fr)	SNR
16	6.8	5.15 ± 0.14	9.9	2.41 ± 0.29
20	14.0	2.62 ± 0.24	19.1	1.54 ± 0.24
24	28.2	1.8 ± 0.3	33.8	1.47 ± 0.19
28	45.4	1.18 ± 0.18	52.6	0.26 ± 0.05

Table 5. Variation of IAK and SNR with FOV for different test objects in DSA and 20 cm of PMMA.

FOV (cm)	LEEDS TOR 18 FG		NEMA XR21	
	IAK (mGy/fr)	SNR	IAK (mGy/fr)	SNR
22	3.40	10.4 ± 0.3	4.0	6.3 ± 0.6
31	1.68	8.7 ± 0.5	2.6	6.9 ± 0.3
42	1.17	8.9 ± 0.5	1.5	5.5 ± 0.6
48	0.90	8.9 ± 0.5	1.1	5.8 ± 0.4

When the simulated patient goes from 16 to 28 cm of PMMA (Table 4), IAK is raised quickly, and in addition SNR values decrease significantly.

For the most common DSA acquisition mode (Table 5), it shows that when magnification is applied, moving from an FOV of 48 to 42, 31 and 22 cm, IAK increases by a factor of 3.7 with both tests and SNR remains almost constant.

DISCUSSION

Additional analysis of the images (e.g. spatial resolution) will be done in a more extended paper. Measurements with the NEMA test object had

bigger errors, due to the characteristics of the circles (they are smaller and have less contrast). Furthermore, in the most adverse conditions, with 28 cm of PMMA or in the low fluoroscopy mode, it is difficult to distinguish any low-contrast detail using this test object.

These results can help to optimise the clinical protocols, especially in the selection of the operation modes and in the use of magnification. Clinicians should know IAK increase factors when moving from low to normal or high fluoroscopy modes (increases of 1.5 or 2.5 for the evaluated system). Magnification improves the high-contrast spatial resolution, but the low contrast sensitivity stays practically constant. The increases in IAK in the evaluated system when moving from 48 to 42, 31 and 22 cm FOV have been factors of 1.5, 1.8 and 2.3, respectively, but the SNR remains practically constant. This is a consequence of the manufacturer settings criteria; to maintain SNR constant when decreasing the number of pixels during magnification, more photons per pixel are needed. Also, the possibility of recording images in fluoroscopy modes can help to substantially reduce patient doses.

REFERENCES

1. Vano, E., Geiger, B. and Schreiner, A. *Dynamic flat panel detector versus image intensifier in cardiac imaging: dose and image quality*. Phys. Med. Biol. **50**, 5731–5742 (2005).
2. http://www.medical.philips.com/main/products/cardiovascular/products/FD20_radio/FD20_radio.html. Accessed 9 April 2007.
3. Faulkner, K. *Introduction to constancy check protocols in fluoroscopic systems*. Radiat. Prot. Dosimetry. **94**(1-2), 65–68 (2001).
4. http://www.leedstestobjects.com/index.php?module_name=products/product_setup&product_name=TOR%2018FG&group_name=Fluoroscopy. Accessed 9 April 2007.
5. Balter, S., Heupler, F. A., Paul Lin, P. J. and Merrill, H. W. *A new tool for benchmarking cardiovascular fluoroscopes. Catheter Cardiovasc. Interv.* **52**(1), 67–72. (2001).
6. http://www.nema.org/stds/complimentary-docs/upload/XR21-NEMA-Instructions.pdf. Accessed 9 April 2007.
7. Hunt, D. C., Tousignant, O. and Rowlands, J. A. *Evaluation of the imaging properties of an amorphous selenium-based flat panel detector for digital fluoroscopy*. Med. Phys. **31**(5), 1166–1175 (2004).
8. Peterzol, A., Padovani, R., Quai, E., Vano, E., Prieto, C. and Aviles, P. *The application of image quality measurements for digital angiography*. Radiat. Prot. Dosimetry. **117**(1–3), 38–43 (2005).
9. Tapiovaara, M. J. and Sandborg, M. *How should low-contrast detail detectability be measured in fluoroscopy*? Med. Phys. **31**(9) 2564–76. (2004)
10. http://www.unfors.com/products.php?catid=19. Accessed 9 April 2007.
11. International Commission on Radiation Units and Measurements. *Patient dosimetry for X rays used in medical imaging*. ICRU Report 74. J. ICRU 5 Medical imaging: The assessment of image quality. ICRU Bethesda, Maryland (2005).
12. www.sim.hcuge.ch/uin Accessed 9 April 2007.
13. Sprawls, P. *Physical principle of medical imaging*. (Madison, WI: Medical Physics Publishing corporation) (1995) ISBN 0 944 838545.